



Published in final edited form as:

Neuroimage. 2014 March ; 88: 271–281. doi:10.1016/j.neuroimage.2013.10.011.

Knowledge-based Automated Reconstruction of Human Brain White Matter Tracts Using a Path-Finding Approach with Dynamic Programming

Muwei Li^{a,b}, J Tilak Ratnanather^{c,d,e}, Michael I. Miller^{c,d,e}, and Susumu Mori^{a,f}

^a The Russell H. Morgan Department of Radiology and Radiological Science, The Johns Hopkins University School of Medicine, Baltimore, MD, USA

^b College of Electronics and Information Engineering, Sichuan University, Chengdu, Sichuan, China

^c Center for Imaging Science, Johns Hopkins University, Baltimore, MD, USA

^c Institute for Computational Medicine, Johns Hopkins University, Baltimore, MD, USA

^c Department of Biomedical Engineering, Johns Hopkins University, Baltimore, MD, USA

^f F. M. Kirby Research Center for Functional Brain Imaging, Kennedy Krieger Institute, Baltimore, MD, USA

Abstract

It has been shown that the anatomy of major white matter tracts can be delineated using diffusion tensor imaging (DTI) data. Tract reconstruction, however, often suffers from a large number of false-negative results when a simple line propagation algorithm is used. This limits the application of this technique to only the core of prominent white matter tracts. By employing probabilistic path-generation algorithms, connectivity between a larger number of anatomical regions can be studied, but an increase in the number of false-positive results is inevitable. One of the causes of the inaccuracy is the complex axonal anatomy within a voxel; however, high-angular resolution (HAR) methods have been proposed to ameliorate this limitation. However, HAR data are relatively rare due to the long scan times required and the low signal-to-noise ratio. In this study, we tested a probabilistic path-finding method in which two anatomical regions with known connectivity were pre-defined and a path that maximized agreement with the DTI data was searched. To increase the accuracy of the trajectories, knowledge-based anatomical constraints were applied. The reconstruction protocols were tested using DTI data from 19 normal subjects to examine test-retest reproducibility and cross-subject variability. Fifty-two tracts were found to be reliably reconstructed using this approach, which can be viewed on our website.

Introduction

White matter tract reconstruction based on diffusion tensor imaging (DTI) was introduced more than 10 years ago (Basser et al., 2000; Conturo et al., 1999; Mori et al., 1999; Poupon et al., 2001). This technique, called tractography, is capable of faithfully reconstructing the

© 2013 Elsevier Inc. All rights reserved

Publisher's Disclaimer: This is a PDF file of an unedited manuscript that has been accepted for publication. As a service to our customers we are providing this early version of the manuscript. The manuscript will undergo copyediting, typesetting, and review of the resulting proof before it is published in its final citable form. Please note that during the production process errors may be discovered which could affect the content, and all legal disclaimers that apply to the journal pertain.

macroscopic architecture of major white matter bundles, but its limitations are also widely known (see, e.g., (Tournier et al., 2011)). The DTI data, in which the neuroanatomy in each pixel is reduced to a mere six parameters, is only an approximation of the tract orientation, assuming all fibers within a voxel are aligned along one orientation. With 2-3 mm resolution, many axons could merge, diverge, or cross within one voxel. In addition, partial voluming occurs in all voxels that are located between two major bundles. As a result, the tractography results are known to have false-positive and false-negative results. To complicate the situation even further, the very notion of various “white matter tracts” was established based on macroscopic visual assessment of postmortem samples (e.g., (Dejerine, 1895; Krieg, 1963)) and their definitions on a microscopic scale, for instance, of the connectivity by axons, are often vague. This ambiguous anatomical definition has led to a lack of gold standards, which makes validation of tractography difficult.

There are several approaches, postulated in the past, to achieve more accurate tractography results. First, we can extract more information from each voxel by not reducing the diffusion information to the six-element tensor model (Frank, 2001, 2002; Tournier et al., 2004; Tuch et al., 2003; Wedeen et al., 2005; Wiegell et al., 2000). These methods usually require two conditions when acquiring data: a large number of diffusion orientation measurements (typically more than 60); and heavy diffusion weighting (typically more than 3,000 s/mm²). From these measurements, the fiber angles of multiple tract populations within a voxel can be estimated. These approaches, however, often sacrifice SNR and higher sensitivity to measurement artifacts, such as subject motion and eddy current. The low SNR of raw images, in particular, makes quality control challenging (Ben-Amitay et al., 2012). The second approach is to improve the tractography method. The simplest approach is deterministic line propagation, which simply follows the principal eigenvector in each voxel (see, e.g., (Mori and Van Zijl, 2002)). This approach has, however, been criticized for its high sensitivity to noise, because it accumulates errors from noise along the path. More elegant probabilistic approaches to incorporate the path uncertainty have also been postulated, in which path generation is repeated under different conditions, leading to multiple potential paths from one seed voxel (Behrens et al., 2003; Jeurissen et al., 2011; Jones, 2003; Jones and Pierpaoli, 2005; Lazar and Alexander, 2003, 2005; Lori et al., 2002; Parker et al., 2002; Richter et al., 2013; Tournier et al., 2002). While these methods can be considered “path generation” approaches, there is another class of “path-finding” approaches, in which the start and end points are prefixed and the most probable path that agrees most with the DTI results is sought. Namely, posing the problem as an optimization problem enables computation of a “shortest path” between chosen initial and terminal points that globally minimizes a sequentially additive energy constraint defined by the tensor in the spirit of the classical Dijkstra’s algorithm (Everts et al., 2009; Fout et al., 2005; Iturria-Medina et al., 2007; Lal, 2004; Lifshits et al., 2009; Merhof et al., 2006a; Merhof et al., 2006b; Poynton et al., 2005; Richter et al., 2013; Tuch et al., 2001; Vorburger et al., 2012; Zalesky, 2008; Zalesky and Fornito, 2009). These assign a probability distribution to the local orientation of fibers at each voxel, and use path finding methods to compute the optimal path between two regions. Our method described in this paper is an extension of these efforts and uses dynamic programming to minimize a quadratic function based on the Gaussian form of the full DTI tensor.

This “path-finding” approach poses a challenging question: “what defines the ground truth where two points are connected?” One can argue that if there is one axon between two points, they are connected. However, we cannot expect that the MRI-based approach can faithfully reconstruct the pathway of a single axon. We could also argue that this approach attempts to reconstruct the large white matter bundles already well-described by classic anatomy literature (Dejerine, 1895; Krieg, 1963). However, visual identification of the long sweep of an axonal bundle from point A to B does not automatically guarantee that these

two points are actually connected; many axons can merge and exit along the pathway and there could be no single axon that travels the entire length of the described tract. These arguments might suggest that tractography is not a tool with which to investigate connectivity based on cellular level structure, but to reconstruct macroscopic white matter architectures or a region-growing tool, which can cluster anatomically related pixels based on DTI data.

Although it is still vague, we could then define our gold standards as those large bundles that have been described by neuroanatomists. Some of the large tracts actually have well known trajectories because their anatomy is homologous to animals, in which invasive studies are possible. These include the corticospinal tract, the visual pathway, the fornix, and many tracts in the brainstem. However, detailed trajectory patterns of many association tracts remain ambiguous because they are much less developed in animals, and our knowledge derived from this method remains at a lobar-level scale. Cortico-thalamic / thalamo-cortical projection fibers, as well as commissural fibers, are subject to the same limitations. A subset of their connectivity patterns are known from animal studies, but our knowledge in the human brain remains at a macroscopic scale; for example, the projection from or to the medial-dorsal thalamic nuclei penetrates the anterior limb of the internal capsule, the frontal corona radiata, and reach the frontal lobe. Assuming that we can use these types of macroscopic knowledge as the gold standards, knowledge-based tractography can effectively increase the precision (reproducibility) of the results, while it also supports the accuracy (validity) of the employed knowledge. Specifically, knowledge-based tractography is usually performed using multiple regions of interest (ROIs) that define at least the two target regions, as well as waypoints along the path (Conturo et al., 1999; Huang et al., 2004). We can use these ROIs as anatomical constraints, retrieving only results that penetrate all the ROIs. Previous analysis has suggested that this approach can reduce false-positives (thus, results are specific), while the false-negatives remain stable (thus, sensitivity is unchanged) when a deterministic approach is used (Huang et al., 2004). In other words, if two target regions, which are known to be a part of a large fiber bundle, are defined in the brain, the reconstructed trajectory, if any, is likely to agree with the known trajectory, but it often returns no result. For example, it is widely known that the projections of the corpus callosum and the projection fibers (e.g., the corticospinal tracts and thalamic radiations) tend to miss large portions of projections to the lateral cortical areas with the tensor model and deterministic approaches.

In this paper, we extended these previous observations by combining a knowledge-based approach with path-finding algorithms. Because path-finding algorithms always generate a path, the false-negatives become zero. If the knowledge-based guidance, as a form of ROIs, ensures removal of false-positives, we expect a highly useful tool with which to study white matter architecture. Of course, the limitation of this logic is that the accuracy is defined by the qualitative anatomical knowledge about the white matter architecture. If we place a large number of ROIs to eliminate all potential false-positive results, the hand-segmented white matter tract, defined by an anatomist and the tractography, is not needed. In this study, therefore, we explored the following questions:

1. Can a path-finding algorithm reconstruct known tract trajectories through ROI guidance? If so, how many ROIs are needed?
2. How does this method compare to conventional deterministic approaches?
3. What is the level of precision in terms of test-retest and cross-subject reproducibility?
4. Can we automate the process of the ROI placement steps?

In this study, we employed the dynamic programming algorithm and tested a pipeline for automated trajectory reconstructions of well-described large white matter bundles to investigate the four questions posed above.

Methods

MRI data

Nineteen healthy volunteers with no history of neurological conditions (10 males, 9 females, 22–61 years old; mean, 31 years old) participated in this study. Local Institutional Review Board approval and written, informed consent were obtained prior to the examination. The details of the protocol can be found elsewhere (Landman et al., 2011). Briefly, the subjects were scanned twice using a 3 T MR scanner (Achieva, Philips Healthcare, Best, The Netherlands). The DTI dataset was acquired with a multi-slice, single-shot, echo-planar imaging (EPI), spin-echo sequence (TR/TE = 6281/67 ms, SENSE factor = 2.5). Sixty-five transverse slices were acquired parallel to the line connecting the anterior commissure (AC) to the posterior commissure (PC), with no slice gap and 2.2 mm nominal isotropic resolution (FOV = 212 × 212, data matrix = 96 × 96, reconstructed to 256 × 256). Diffusion weighting was applied along 32 directions (Philips parameters: gradient overplus = no, directional resolution = high, gradient mode = enhanced) with a b -value of 700 s/mm². Five minimally weighted images (five B_0 with $b \approx 33$ s/mm²) were acquired and averaged on the scanner as part of each DTI dataset. The total scan time to acquire the DTI dataset was 4 min 11 s. No cardiac or respiratory gating was employed.

The raw diffusion-weighted images (DWIs) were first co-registered to one of the b_0 images and corrected for eddy current and subject motion with affine transformation using Automated Image Registration (AIR) (Woods et al., 1998). The six elements of the diffusion tensor were calculated for each pixel with multivariate linear fitting using DtiStudio (Jiang et al., 2006). After diagonalization, three eigenvalues and eigenvectors were obtained. For the anisotropy map, fractional anisotropy (FA) was used (Pierpaoli et al., 1996).

LDDMM-based parcellation

We used a single-subject white matter atlas (JHU-MNI-ss, www.mristudio.org) in the ICBM-152/ICBM-DTI-81 space. A detailed description of this atlas can be found in (Oishi et al., 2009). A two-step image transformation was used to warp the atlas to individual data. First, affine transformation was used to globally adjust the brain position, rotation, and the size. Then, a non-linear transformation using LDDMM (Large Deformation Diffieomorphic Metric Mapping) was applied. For LDDMM, the dual-contrast LDDMM was used (Ceritoglu et al., 2009) in which both the b_0 image and the FA map were used simultaneously. These procedures are reciprocal and provide forward (subject → atlas) and backward (atlas → subject) transformation matrices.

Automated reconstruction of human brain white matter

The automated reconstruction began with the definition of at least two regions of interest (ROIs) identifying two connected brain regions. We followed our previous publication to define the ROIs in an automated manner (Zhang et al., 2008; Zhang et al., 2010). Briefly, the JHU-MNI-ss atlas contains pre-parcellated structural definition files (brain parcellation map (BPM)). One of these BPMs, called a Type II BPM, contains 130 parcellated structures, which was warped to all subjects using the backward transformation matrices. For each tract of interest, two seed parcels in the BPM were defined as ROIs to drive the tractography, exploiting the existing anatomical knowledge of tract trajectories. Additional “AND” (waypoint) ROIs were also selected from the BPM to pose anatomical constraints (reconstructed tracts must penetrate these ROIs). Depending on the tracts, additional “NOT”

parcels had to be defined to remove frequently occurring false-positives (all tracts that penetrate these ROIs are removed). In this way, the anatomical knowledge about the known trajectory of each tract was stored as seed ROIs, waypoint ROIs, and NOT ROIs inside the BPM. We generated the BPM for 52 white matter tracts, which were transformed to each subject using the backward transformation matrix for the automated tract reconstruction. The names of the reconstructed tracts and parcels used for ROIs are displayed in Table 1.

Tractography methods

Two types of tractography approaches were used. First, the conventional streamline propagation was performed, using an algorithm called Fiber Assignment by Continuous Tracking (FACT), which simply follows the orientation of the principal eigenvector (Mori et al., 1999). For FACT, we used $FA > 0.25$, and transition angles < 30 degrees were used for thresholds. Second, the path-finding approach was performed by dynamic programming (Khaneja et al., 1998; Qiu et al., 2006; Ratnanather et al., 2003). The detail of the white matter tract generation by dynamic programming is provided by (Ratnanather et al., 2013).

Briefly, this algorithm finds the optimal path between two seed regions by searching over all possible paths that connect them. A cost function, in the form of probability distribution on fiber tract orientation, was set to each point on the path, representing the probabilities of the transitions between the point and each of its 26 neighbors. Dynamic programming was used to calculate the linking with the lowest cumulative cost of all points on the path. Let λ_1^i, λ_2^i and λ_3^i be the eigenvalues of tensor D_i normalized by its trace at point i , and e_1^i, e_2^i and e_3^i be the unit eigenvectors of D_i , the cost function for point i transiting along orientation d_j , which is given by:

$$\pi(i, j) = \|d_j\|^2 \left(\frac{\langle \bar{d}_j, e_1^i \rangle}{\lambda_1^i} + \frac{\langle \bar{d}_j, e_2^i \rangle}{\lambda_2^i} + \frac{\langle \bar{d}_j, e_3^i \rangle}{\lambda_3^i} \right) + \ln(\lambda_1^i \lambda_2^i \lambda_3^i) + 3 \ln(2\pi)$$

where $\bar{d}_j = d_j / \|d_j\|$ is the unit directional vector indicating the transiting orientation. The constant term ensures the positivity of the function. In implementation, a threshold was used to eliminate fibers passing through high isotropic areas by setting $\pi(i, j) = 10000$ when $FA < 0.25$.

After the path finding, a knot vector $K = k_i$ was obtained recording the coordinates of voxels along the “blocky” path. Then a smooth streamline was represented by connecting sections of continuous points $p(t_j)$ where each section of points $p_i(t_j)$ was estimated by b-spline function of the knot k_i . In our implementation, equidistant cubic b-spline function was used, whose matrix expression is shown:

$$p_i(t_j) = \frac{1}{6} \begin{bmatrix} t_j^1 & t_j^2 & t_j^3 \end{bmatrix} \begin{bmatrix} -1 & 3 & -3 & 1 \\ 3 & -6 & 3 & 0 \\ -3 & 0 & 3 & 0 \\ 1 & 4 & 1 & 0 \end{bmatrix} \begin{bmatrix} k_i \\ k_{i+1} \\ k_{i+2} \\ k_{i+3} \end{bmatrix}$$

Where $t_j, [0:0.05:1]$, which means 20 equidistant and continuous points were used for representing the section of curve. The calculation was performed on a desktop with Intel Xeon 2.13GHz CPU (4 core, 4 thread). The computation load is 2.17s/streamline using a single CPU core. Employment of four parallel processing reduced the time to 0.54s/streamline.

After fibers were generated by the initial seed ROI-ROI tracking, and the logical operations "AND" and "NOT" were applied on the fibers. This is an "editing" process aimed at selecting fibers passing through the anatomically known areas. One of the important limitations of dynamic programming is that the size of the ROI needs to be small with respect to the level of the anatomical resolution. For example, if we define the entire motor cortices in both hemispheres and find paths connecting the two ROIs, the path-finding method would report only trajectories that connect the closest regions; for example the right medial motor cortex to the left medial motor cortex. The long paths connecting lateral regions of the motor cortices inevitably have higher costs. Anatomically, it is known that most cortical areas have commissural connections to homotopic areas in the opposite hemisphere. Although connections to heterotopic areas are also known, we used anatomical constraints for the reconstruction of the homotopic areas. This was achieved by dividing the cortical ROIs into 27-voxel (3*3*3) sub-parcels, and the connections between two corresponding sub-parcels from both hemispheres were reconstructed. The "corresponding" sub-parcels were found by determining the closest sub-parcel after a reflection operation about a midline. For projection fibers (connecting a cortical parcel and a non-cortical parcel), multiple trajectories between a non-cortical parcel and each 27-voxel sub-parcels in the cortical areas were reconstructed.

Reproducibility evaluation

The precision (reproducibility) of this automated tractography method was evaluated using an intra-subject test-retest reproducibility; namely, the same tracts were reconstructed automatically using the fiber-finding algorithm using two sets of DTI data from the 19 selected subjects scanned on different dates. We used the reconstructed results from the pontine tracts for the reproducibility study because they are the most challenging due to the long lengths and convoluted trajectories. The reproducibility of the two trials was measured by mean along-tract FA values and by streamline distances. Two corresponding paths which connected same destinations were first converted to two smooth streamlines by b-spline interpolation. Then equal numbers of control points were uniformly sampled respectively on these two streamlines where these control points were indexed from 1 to N. The average distance of all N pairs of corresponding control points was calculated and used as the streamline distance.

Creation of probabilistic atlases

To create probabilistic coordinates of various white matter tracts reconstructed in this study, the tractography results were first converted to binary image files (1: voxels that contain the tracts, 0: the remaining voxels), which were then transformed to the reference atlas using the LDDMM forward transformation matrices. The binary files from the 19 normal subjects were then averaged to create probabilistic maps in the MNI coordinates.

Availability of the code

The matlab scripts, together with the command-line executable files which performed the tracking, can be downloaded from www.mristudio.org.

Results

Commissural fibers

Fig. 1A and 1B compare results from the dynamic programming and the conventional deterministic method, in which commissural connections between the right and left pre-central gyri (PrCGs) are shown. As is widely known, the deterministic approach could reconstruct only the projections to the medial homotopic areas. Dynamic programming used

the two seed parcels (red parcels in Fig. 1A) and one waypoint parcel defining the corpus callosum at the mid-sagittal level (the blue parcel in Fig. 1A), from which the algorithm found connection pathways penetrating the corpus callosum. Dynamic programming revealed the trajectories to the lateral regions. The cortical regions were divided into 18 regions, as shown in Table 1, and 18 commissural connection patterns were defined. Of these connections, the connections between four parcels in the temporal lobe were reconstructed; all the generated tracts did not conform to the anatomical criteria posed by the ROIs (Table 1). In Fig. 1C, the commissural connections of 18 connected areas are shown (only five colors are assigned, grouping the 18 fibers based on the connections to the five lobes for visualization purposes).

Thalamus-cortex connections

The parcel combinations designed for the thalamus-cortex (thalamocortical and corticothalamic) connections are tabulated in Table 1. Fig. 2 shows several thalamic projection tracts generated by the dynamic programming, including the ventroposterior nucleus to the post-central gyrus, the mediodorsal nucleus to the prefrontal lobe/orbital gyrus, and the ventrolateral nucleus to the inferior frontal gyrus. The connections between the specific thalamic nuclei and the cortical areas are well-described from past histological studies, and the combinations of these parcels were based on this knowledge. However, we would like to point out that there were sets of connections that have been described in the past, but dynamic programming could not find consistent paths among the 19 subjects. These included connections between the anterior nucleus and the cingulate gyrus, the lateral geniculate nucleus (LGN) and the cuneus, the superior occipital gyrus, the pulvinar and the cuneus, the precuneus, the lingual gyrus, and the superior occipital gyrus, which have tortuous trajectories. The results of the LGN – visual cortex tracking from the 19 subject are shown in Fig. 3 as a demonstration of the failure. In this population-averaged map, it can be seen that, approximately half of the streamlines have shorter and erroneous paths. The comparison with FACT is not shown because FACT returned null results for many of these connections.

Corticospinal tracts

Although many cortical areas are known to have projections to the brainstem, we reconstructed only the projections from the motor cortex. Fig. 4A/4B and 4C/4D show the reconstruction results for the corticospinal tract using the dynamic programming and FACT. It is widely known that deterministic approaches fail to reveal connections to the lateral cortex, as shown in Fig. 4C and 4D. The lateral connections delineated by the dynamic programming method agreed with the anatomical knowledge; they penetrate the corona radiata and the posterior limb of the internal capsule (Fig. 4B).

Corticopontine tracts

It is known that all cortical regions have connections to the pons and they all penetrate the cerebral peduncle. Fig. 5 shows the reconstruction results from the cerebral peduncle (1st seed parcel) to 17 defined cortical areas (2nd seed parcel). However, dynamic programming failed to find consistent connections to two posterior regions of the hemisphere among the 19 subjects, including the precuneus and the superior occipital gyrus.

Test-retest reproducibility and population averages

The reproducibility of FA measurements was performed by superimposing each trial result on the FA maps. The results of two trials for 18 pontine tracts (total of 36 for both hemispheres) are shown in Fig. 6, in which the error bars indicate standard deviations in the 19 healthy subjects. The average coefficients of variance (standard deviation/average) of the

FA values over 19 subjects (cross-subject variability) were $4.5\% \pm 2.2\%$. The average test-retest difference was $0.6\% \pm 0.5\%$ over the 36 tracts. The average streamline distances over 19 subjects were $2.62 \pm 0.74\text{mm}$, slightly larger than the pixel size (2.2mm) (Fig. 7). There were no tracts with more than a two-pixel distance, on average, although there were several tracts (CP_CU_L, CP_CU_R, CP_FU_L, CP_LG_L, and CP_PrCU_L) in which the distances reached three pixels in some subjects.

Probabilistic tract atlases based on the dynamic programming results

Fig. 8 shows probabilistic atlases of the pontine tracts in the MNI coordinates. The 18 pontine tracts are combined into five groups based on their projections to five different lobes for visualization purposes.

Discussion

In this study, we applied a path-finding algorithm to reconstruct various known white matter tracts using conventional DTI data. Our algorithm is based on dynamic programming, which determines the optimal path between the beginning and destination parcels by efficiently searching over all paths that connect the seed parcels and identifying the path that has the lowest cumulative cost of all points along the path.

In previous studies, the limitations of deterministic tract reconstruction approaches, combined with DTI, have been widely discussed. The line propagation by the deterministic approach relies on several thresholds; the degrees of FA and curvature are most commonly used. When the line propagation is applied to brain regions with complicated fiber anatomy, it tends to be terminated by the thresholds due to decreased FA or sharp angle transitions (false-negative). Depending on the fiber angles of the multiple fiber populations, the propagation could continue following artificial “averaged” fiber angles (false-positive). If this method is combined with the ROI-driven, knowledge-based approach, we often find that there are no connections between the two specified regions that are known to be connected, because the propagation is either terminated on the way or deviated from the real path and could not reach the multiple specified ROIs. The most notable limitation is the lack of trajectories of the commissural and projection fibers that reach to the lateral cortical regions. This is believed to be due to the large association fibers running along the anterior-posterior orientations, erasing the anatomical information of the lesser commissural and projection fiber populations running along the lateral orientations.

It has been shown that these lateral trajectories can be reconstructed by using HARDI-type data acquisition and data processing, such as diffusion spectrum imaging (DSI), Q-ball imaging, or spherical harmonic deconvolution (see, e.g., a recent review by (Tournier et al., 2011)). These methods potentially would provide more accurate information about tract trajectories. However, there are important practical disadvantages to these approaches. First, the HARDI acquisition usually uses more than 60 diffusion-encoding orientations, which would typically require at least seven-to-eight minutes of scan time, while many clinical DTI can afford only five minutes or less. The higher the number of orientations, the more difficult it becomes to incorporate into routine scans. More importantly, b-values are required to be at least $3,000 \text{ s/mm}^2$ and as high as $30,000 \text{ s/mm}^2$. This would lead to a substantial amount of signal loss and, thus, a lower SNR. The high b-value also requires a longer echo time, which further reduces the SNR. Higher degrees of eddy current and motion artifacts are also troublesome, which are difficult to correct due to the poor SNR of the raw images. To improve the poor SNR, HARDI acquisition typically employs a much a longer scan time (signal averaging) and a lower spatial resolution. Due to these practical difficulties, the majority of diffusion studies currently rely on conventional DTI protocols with a smaller number of diffusion-weighting orientations (< 30) and smaller b-values ($<$

1,000 s/mm²). Our approach, which is based on the conventional DTI data, therefore, has practical importance.

One important question about the combination of the DTI and a path-finding approach is whether the results are accurate (i.e., validity). To evaluate the accuracy, we need to define a gold standard. The difficulty of the validation of tractography stems from the ambiguity of the gold standard. MRI signals are based on voxel-by-voxel-averaged properties of water molecules. The voxel-by-voxel DTI information and tractography results depend on imaging parameters, such as image resolution, employed b-values, and signal-to-noise. Even if the same object is scanned, different imaging parameters would lead to different results, while the underlying neuroanatomy remains the same. MRI-based methods obviously cannot observe a single-neuron connection. We could define “brain connectivity” as the biological target of the study, but the notion of “connectivity” is vague and difficult to establish as a gold standard against which accuracy could be measured.

In this study, we consider tractography by dynamic programming as a region-growing or segmentation tool with which a group of voxels are defined that are estimated to belong to a white matter bundle of interest. This can also be considered a brain-mapping tool, with which a group of equivalent voxels is defined across different subjects. The defined voxels by this approach are related to the existing anatomical knowledge, and therefore, can be linked to a body of literature about their anatomy and functions. This is possible because the reconstruction is guided by the ROI sets defined in the BPM, based on the existing anatomical knowledge. Of course, this is an assumption that may not hold for severe pathological cases, in which the trajectory of the tract of interest is altered. For example, even if a tract is destroyed by stroke or tumor, the dynamic programming still identifies a path. Therefore, this approach should be applied only to cases with a mild amount of pathology.

If this approach is valid, then an important question is its reliability as a tool. The tool would be reliable if it has a high level of precision (test-retest reproducibility). The tool also has the potential to be a sensitive tool if the variability among the normal subjects is small, and thus, it would have a high statistical power to detect cross-subject differences.

The test-retest reproducibility of the tract reconstruction by dynamic programming was measured in terms of FA value, and tract distances between two trials. The spatial reproducibility and FA values of test-retest results were excellent; within one pixel for spatial reproducibility, and 0.6% for FA values. However, there were four tracts that on average deviated by more than 4 mm. We consider the test-retest reproducibility of these tracts fair. For cross-subject variability among the normal population, the FA measures have a 4.5% variability, on average, and again, the values depend heavily on the tract of interest. As expected, the tracts with a large amount of variability in spatial matching, such as the corticopontine tracts from CU, LG, PrCU, and SPG, tend to have larger cross-subject variability in the FA values. This could be due to the more tortuous trajectories of these tracts and the resultant decrease in measurement reproducibility, but we cannot deny the possibility of real biological variability among the subjects.

There are several ways to apply this automated tractography tool to actual studies. First, the tract reconstruction can be applied to each subject to obtain subject-specific reconstruction results, from which tract size and voxel properties (e.g., FA, MD, and other diffusivity measures) can be measured. Conversely, the probabilistic atlas can be applied to each subject, from which affected tracts can be estimated.

Conclusion

In conclusion, we developed a new automated tractography tool using a path-finding algorithm. The reconstruction is driven by anatomical knowledge stored in the BPM, which is warped to each subject's data. A total of 52 tracts were reconstructed using this approach. The reconstruction was repeated using data from two repeated measurements of 19 healthy subjects. A high level of test-retest reproducibility was observed. Tract-specific FA values were measured from the 19 subjects, and a small degree of variability was found. The reconstruction results of 52 tracts from the 19 subjects were normalized to the MNI coordinates and probabilistic maps were created. The BPMs for the automated reconstructions of the 52 tracts and reconstruction results in the MNI space are available for download from www.mristudio.org. The proposed tool and the atlases (both the BPM and probabilistic coordinates) could be useful resources for tract-specific anatomical evaluation of brain MRI.

References

- Basser PJ, Pajevic S, Pierpaoli C, Duda J, Aldroubi A. In vitro fiber tractography using DT-MRI data. *Magn. Reson. Med.* 2000; 44:625–632. [PubMed: 11025519]
- Behrens TE, Johansen-Berg H, Woolrich MW, Smith SM, Wheeler-Kingshott CA, Boulby PA, Barker GJ, Sillery EL, Sheehan K, Ciccarelli O, Thompson AJ, Brady JM, Matthews PM. Non-invasive mapping of connections between human thalamus and cortex using diffusion imaging. *Nat Neurosci.* 2003; 6:750–757. [PubMed: 12808459]
- Ben-Amitay S, Jones DK, Assaf Y. Motion correction and registration of high b-value diffusion weighted images. *Magn Reson Med.* 2012; 67:1694–1702. [PubMed: 22183784]
- Ceritoglu C, Oishi K, Li X, Chou MC, Younes L, Albert M, Lyketsos C, van Zijl PC, Miller MI, Mori S. Multi-contrast large deformation diffeomorphic metric mapping for diffusion tensor imaging. *Neuroimage.* 2009; 47:618–627. [PubMed: 19398016]
- Conturo TE, Lori NF, Cull TS, Akbudak E, Snyder AZ, Shimony JS, McKinstry RC, Burton H, Raichle ME. Tracking neuronal fiber pathways in the living human brain. *Proc. Natl. Acad. Sci. USA.* 1999; 96:10422–10427. [PubMed: 10468624]
- Dejerine, J. Anatomie des centres nerveux. Rueff; Paris: 1895.
- Everts, MH.; Bekker, H.; Roerdink, JBTM. Visualizing White Matter Structure of the Brain using Dijkstra's Algorithm. In: Zinterhof, P.; Lonari, S.; Uhl, A.; Carini, A., editors. Proc. 6th International Symposium on Image and Signal Processing and Analysis (ISPA 2009); Salzburg, Austria. 2009. p. 575-580.
- Fout, N.; Huang, J.; Ding, Z. Visualization of neuronal fiber connections from DT-MRI with global optimization. SAC '05: Proc. 2005 ACM Symp. Applied Computing; 2005. p. 1200-1206. ACM Press
- Frank LR. Anisotropy in high angular resolution diffusion-weighted MRI. *Magn Reson Med.* 2001; 45:935–939. [PubMed: 11378869]
- Frank LR. Characterization of anisotropy in high angular resolution diffusion-weighted MRI. *Magn Reson Med.* 2002; 47:1083–1099. [PubMed: 12111955]
- Huang H, Zhang J, van Zijl PC, Mori S. Analysis of noise effects on DTI-based tractography using the brute-force and multi-ROI approach. *Magn Reson Med.* 2004; 52:559–565. [PubMed: 15334575]
- Iturria-Medina Y, Canales-Rodriguez EJ, Melie-Garcia L, Valdes-Hernandez PA, Martinez-Montes E, Aleman-Gomez Y, Sanchez-Bornot JM. Characterizing brain anatomical connections using diffusion weighted MRI and graph theory. *NeuroImage.* 2007; 36:645–660. [PubMed: 17466539]
- Jeurissen B, Leemans A, Jones DK, Tournier JD, Sijbers J. Probabilistic fiber tracking using the residual bootstrap with constrained spherical deconvolution. *Hum Brain Mapp.* 2011; 32:461–479. [PubMed: 21319270]
- Jiang H, van Zijl PC, Kim J, Pearlson GD, Mori S. DtiStudio: resource program for diffusion tensor computation and fiber bundle tracking. *Comput Methods Programs Biomed.* 2006; 81:106–116. [PubMed: 16413083]

- Jones DK. Determining and visualizing uncertainty in estimates of fiber orientation from diffusion tensor MRI. *Magn Reson Med.* 2003; 49:7–12. [PubMed: 12509814]
- Jones DK, Pierpaoli C. Confidence mapping in diffusion tensor magnetic resonance imaging tractography using a bootstrap approach. *Magn Reson Med.* 2005; 53:1143–1149. [PubMed: 15844149]
- Khaneja N, Miller MI, Grenander U. Dynamic programming generation of geodesics and sulci on brain surfaces. *IEEE Trans. on Pattern Analysis and Machine Intelligence.* 1998; 20:1260–1265.
- Krieg, W. *Connections of the cerebral cortex.* Brain books; Evanston, IL: 1963.
- Lal, RM. *Tracking in Diffusion Tensor Imaging.* The Johns Hopkins University; 2004.
- Landman BA, Huang AJ, Gifford A, Vikram DS, Lim IA, Farrell JA, Bogovic JA, Hua J, Chen M, Jarso S, Smith SA, Joel S, Mori S, Pekar JJ, Barker PB, Prince JL, van Zijl PC. Multi-parametric neuroimaging reproducibility: a 3-T resource study. *Neuroimage.* 2011; 54:2854–2866. [PubMed: 21094686]
- Lazar M, Alexander AL. An error analysis of white matter tractography methods: synthetic diffusion tensor field simulations. *NeuroImage.* 2003; 20:1140–1153. [PubMed: 14568483]
- Lazar M, Alexander AL. Bootstrap white matter tractography (BOOT-TRAC). *Neuroimage.* 2005; 24:524–532. [PubMed: 15627594]
- Lifshits S, Tamir A, Assaf Y. Combinatorial fiber-tracking of the human brain. *NeuroImage.* 2009; 48:532–540. [PubMed: 19501657]
- Lori NF, Akbudak E, Shimony JS, Cull TS, Snyder AZ, Guillory RK, Conturo TE. Diffusion tensor fiber tracking of human brain connectivity: acquisition methods, reliability analysis and biological results. *NMR Biomed.* 2002; 15:494–515. [PubMed: 12489098]
- Merhof, D.; Enders, F.; Hastreiter, P.; Ganslandt, O.; Fahlbusch, R.; Nimsky, C.; Stamminger, M. Neuronal fiber connections based on A*-pathfinding. In: Manduca, A.; Amini, AA., editors. *Medical Imaging 2006: Physiology, Function, and Structure from Medical Images.* SPIE; San Diego, CA, USA: 2006a. p. 61431S-61438.
- Merhof D, Richter M, Enders F, Hastreiter P, Ganslandt O, Buchfelder M, Nimsky C, Greiner G. Fast and accurate connectivity analysis between functional regions based on DT-MRI. *LNCS.* 2006b; 4191:225–233.
- Mori S, Crain BJ, Chacko VP, van Zijl PCM. Three-dimensional tracking of axonal projections in the brain by magnetic resonance imaging. *Ann Neurol.* 1999; 45:265–269. [PubMed: 9989633]
- Mori S, Van Zijl PC. Fiber tracking: principles and strategies - a technical review. *NMR Biomed.* 2002; 15:468–480. [PubMed: 12489096]
- Oishi K, Faria A, Jiang H, Li X, Akhter K, Zhang J, Hsu JT, Miller MI, van Zijl PC, Albert M, Lyketos CG, Woods R, Toga AW, Pike GB, Rosa-Neto P, Evans A, Mazziotta J, Mori S. Atlas-based whole brain white matter analysis using Large Deformation Diffeomorphic Metric Mapping: Application to normal elderly and Alzheimer's disease participants. *Neuroimage.* 2009
- Parker GJ, Wheeler-Kingshott CA, Barker GJ. Estimating distributed anatomical connectivity using fast marching methods and diffusion tensor imaging. *IEEE Trans Med Imaging.* 2002; 21:505–512. [PubMed: 12071621]
- Pierpaoli C, Jezzard P, Basser PJ, Barnett A, Di Chiro G. Diffusion tensor MR imaging of the human brain. *Radiology.* 1996; 201:637–648. [PubMed: 8939209]
- Poupon C, Mangin J, Clark CA, Frouin V, Regis J, Le Bihan D, Bloch I. Towards inference of human brain connectivity from MR diffusion tensor data. *Med Image Anal.* 2001; 5:1–15. [PubMed: 11231173]
- Poynton, C.; Lal, R.; Ratnanather, JT.; Mori, S.; Boatman, D.; Miller, MI. Probabilistic Tracking of Fiber Pathways Using Dynamic Programming. *Human Brain Mapping Conference;* Toronto: 2005.
- Qiu A, Rosenau BJ, Greenberg AS, Hurdal MK, Barta P, Yantis S, Miller MI. Estimating linear cortical magnification in human primary visual cortex via dynamic programming. *Neuroimage.* 2006; 31:125–138. [PubMed: 16469509]
- Ratnanather JT, Barta PE, Honeycutt NA, Lee N, Morris HM, Dziorny AC, Hurdal MK, Pearlson GD, Miller MI. Dynamic programming generation of boundaries of local coordinatized submanifolds in the neocortex: application to the planum temporale. *Neuroimage.* 2003; 20:359–377. [PubMed: 14527596]

- Richter M, Zolal A, Ganslandt O, Buchfelder M, Nimsy C, Merhof D. Evaluation of diffusion-tensor imaging-based global search and tractography for tumor surgery close to the language system. *PLoS One*. 2013; 8:e50132. [PubMed: 23308093]
- Tournier JD, Calamante F, Gadian DG, Connelly A. Direct estimation of the fiber orientation density function from diffusion-weighted MRI data using spherical deconvolution. *Neuroimage*. 2004; 23:1176–1185. [PubMed: 15528117]
- Tournier JD, Calamante F, King MD, Gadian DG, Connelly A. Limitations and requirements of diffusion tensor fiber tracking: an assessment using simulations. *Magn Reson Med*. 2002; 47:701–708. [PubMed: 11948731]
- Tournier JD, Mori S, Leemans A. Diffusion tensor imaging and beyond. *Magn Reson Med*. 2011; 65:1532–1556. [PubMed: 21469191]
- Tuch DS, Reese TG, Wiegell MR, Wedeen VJ. Diffusion MRI of complex neural architecture. *Neuron*. 2003; 40:885–895. [PubMed: 14659088]
- Tuch, DS.; Wiegell, MR.; Reese, TG.; Belliveau, JW.; Wedeen, V. Proceeding of International Society of Magnetic Resonance in Medicine. Glasgow, UK: 2001. Measuring cortico-cortical connectivity matrices with diffusion spectrum imaging; p. 502
- Vorburger RS, Reischauer C, Boesiger P. BootGraph: Probabilistic fiber tractography using bootstrap algorithms and graph theory. *Neuroimage*. 2012; 66C:426–435. [PubMed: 23110883]
- Wedeen VJ, Hagmann P, Tseng WY, Reese TG, Weisskoff RM. Mapping complex tissue architecture with diffusion spectrum magnetic resonance imaging. *Magn Reson Med*. 2005; 54:1377–1386. [PubMed: 16247738]
- Wiegell M, Larsson H, Wedeen V. Fiber crossing in human brain depicted with diffusion tensor MR imaging. *Radiology*. 2000; 217:897–903. [PubMed: 11110960]
- Woods RP, Grafton ST, Holmes CJ, Cherry SR, Mazziotta JC. Automated image registration: I. General methods and intrasubject, intramodality validation. *J Comput Assist Tomogr*. 1998; 22:139–152.
- Zalesky A. DT-MRI fiber tracking: a shortest paths approach. *IEEE Trans Med Imaging*. 2008; 27:1458–1471. [PubMed: 18815098]
- Zalesky A, Fornito A. A DTI-derived measure of cortico-cortical connectivity. *IEEE Trans Med Imaging*. 2009; 28:1023–1036. [PubMed: 19150781]
- Zhang WH, Olivi A, Hertig SJ, van Zijl P, Mori S. Automated fiber tracking of human brain white matter using diffusion tensor imaging. *Neuroimage*. 2008; 42:771–777. [PubMed: 18554930]
- Zhang YJ, Zhang JY, Oishi K, Faria AV, Jiang HY, Li X, Akhter K, Rosa-Neto P, Pike GB, Evans A, Toga AW, Woods R, Mazziotta JC, Miller MI, van Zijl PCM, Mori S. Atlas-guided tract reconstruction for automated and comprehensive examination of the white matter anatomy. *Neuroimage*. 2010; 52:1289–1301. [PubMed: 20570617]

Highlights

- Dynamic programming (DP) was applied to tractography based on DTI data.
- DP finds the most probable path between two specified brain regions.
- DP delineates large tracts that could not be reconstructed by streamline methods.
- For accurate path generation, knowledge-based ROI sets are built.
- Fifty two tracts were reconstructed in the MNI space for white matter atlases.

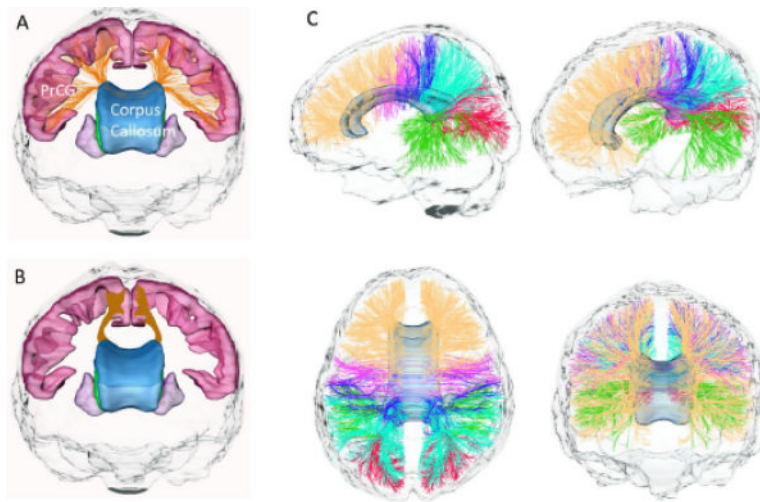


Fig 1. Comparison of commissural fibers reconstructed by dynamic programming (Fig 1A) and the conventional deterministic method (Fig 1B) in the coronal view. The corpus callosum, pre-central gyri, putamen, and caudate were visualized as landmarks. Fig 1C: Visualization of commissural fibers of six connected lobes, including the frontal lobe (wheat), pre-central gyrus (hot pink), post-central gyrus (blue), parietal lobe (cyan), occipital lobe (red), and temporal lobe (green). The temporo-temporal fibers did not conform to the anatomical criteria.

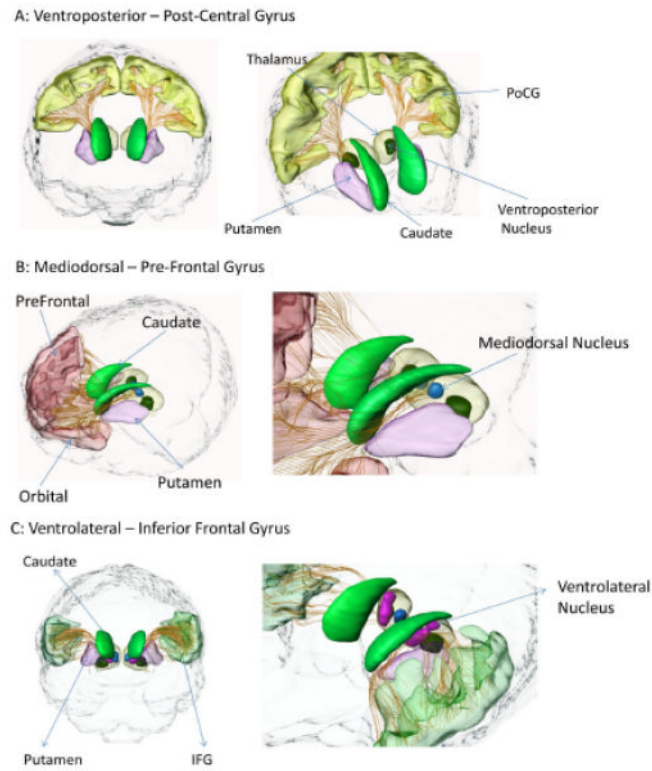


Fig 2. Three thalamic projection tracts generated by the dynamic programming. Fig 2A: Connection between the ventro-posterior nucleus and the post-central gyrus. Fig 2B: Connection between the medio-dorsal nucleus and the pre-frontal gyrus. Fig 2C: Connection between the ventro-lateral nucleus and the inferior frontal gyrus. The thalamus, putamen, caudate, and connected cortical areas were visualized as landmarks.



Fig 3.
Population-average results of the LGN – visual cortex.

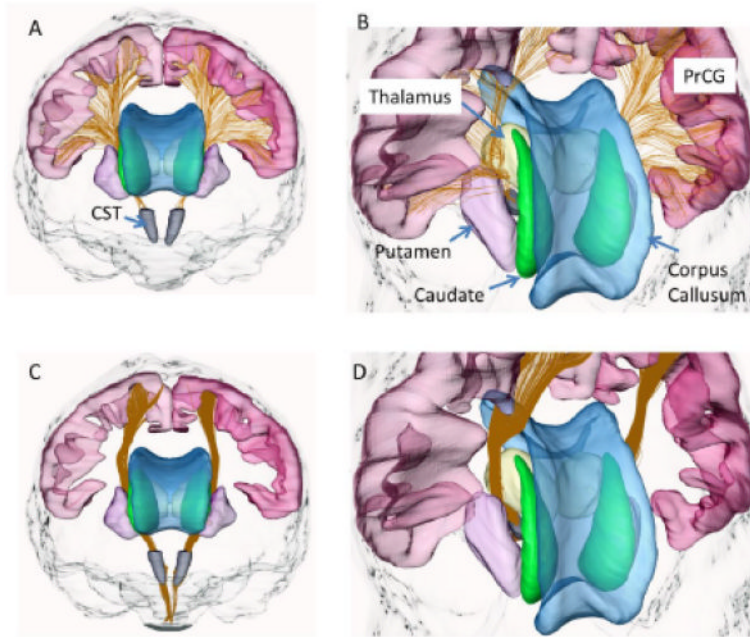


Fig 4. Comparison of the cortico-spinal tract reconstructed by dynamic programming (Fig 3A and 3B) and the conventional deterministic method (Fig 3C and 3D). The CST, thalamus, putamen, caudate, corpus callosum, and pre-central gyri were visualized as landmarks.

Cerebral peduncle – Cortex: all fiber with different colors for 6 lobes.

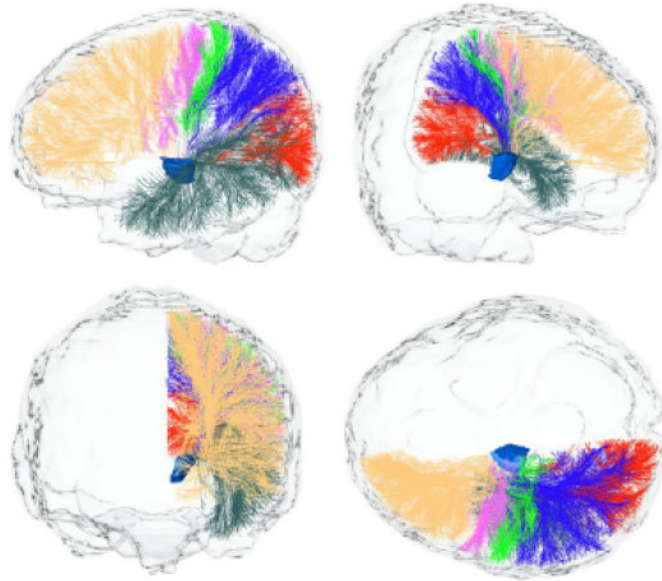


Fig 5. Visualization of cortico-pontine tracts connecting the cerebral peduncle and six brain lobes, including the frontal lobe (wheat), the pre-central gyrus (hot pink), the post-central gyrus (lime), the parietal lobe (blue), the occipital lobe (red), and the temporal lobe (dark green). The cerebral peduncle (blue surface) was visualized as the seed area.

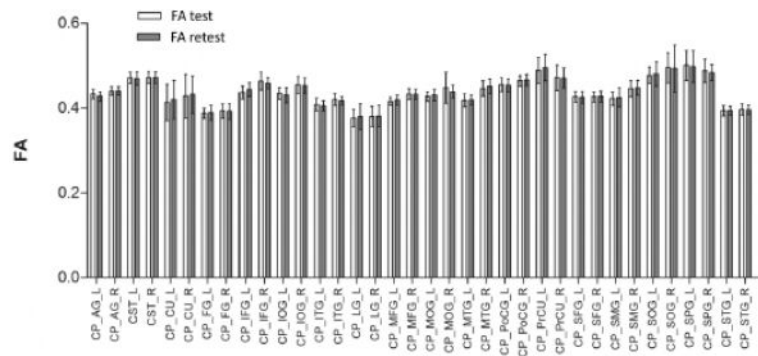


Fig 6. Reproducibility of FA measurements between two trials for 18 pontine tracts (total of 36 for both hemispheres). Error bars indicate standard deviations for 19 healthy subjects.

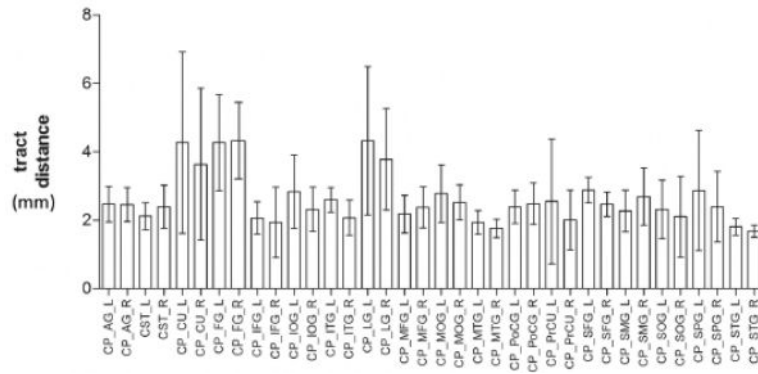


Fig 7. Average streamline distances between two trials for 18 pontine tracts (total of 36 for both hemispheres). Error bars indicate standard deviations of test-retest streamline distances over 19 healthy subjects.

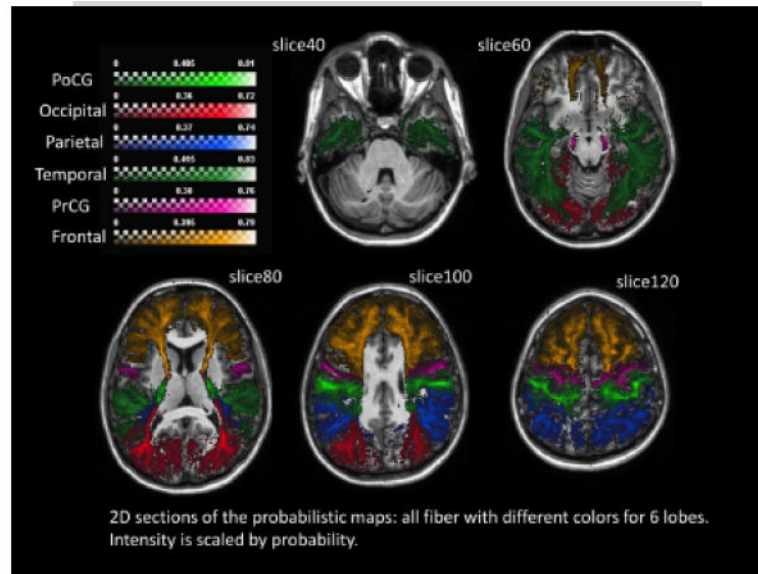


Fig 8. Two-dimensional sections of the probabilistic maps of the cortico-pontine tracts. Spatial probabilities of six tracts, which respectively spread to six brain lobes, are represented by six color bars.

Table 1

Names of reconstructed tracts and ROI sets for guiding the tracking.

Tract Name	1 st ROI	2 nd ROI	Waypoint ROI	NOT ROIs
CC1	AG_L	AG_R	CC	-
CC2	PrCG_L	PrCG_R	CC	-
CC3	CU_L	CU_R	CC	-
CC4	FU_L	FU_R	SCC	GCC, BCC
CC5	IFG_L	IFG_R	CC	-
CC6	IOG_L	IOG_R	CC	-
CC7	ITG_L	ITG_R	SCC	GCC, BCC
CC8	LG_L	LG_R	CC	-
CC9	MFG_L	MFG_R	CC	-
CC10	MOG_L	MOG_R	CC	-
CC11	MTG_L	MTG_R	SCC	GCC, BCC
CC12	PoCG_L	PoCG_R	CC	-
CC13	PrCU_L	PrCU_R	CC	-
CC14	SFG_L	SFG_R	CC	-
CC15	SMG_L	SMG_R	CC	-
CC16	SOG_L	SOG_R	CC	-
CC17	SPG_L	SPG_R	CC	-
CC18	STG_L	STG_R	SCC	GCC, BCC
TR1	LGB	IOG	-	Contralateral hemisphere, LG, SCC, cerebellum, MOG, FU, ITG, MTG
TR2	LGB	LG	-	Contralateral hemisphere, cerebellum, SCC, MOG, IOG, Cu, PCC
TR3	LGB	MOG	-	Contralateral hemisphere, SOG, SCC, LG, FU, AG, Cu, MTG
TR4	MD	OG	-	Contralateral hemisphere, Caud, Put, IFO, Ins, STG
TR5	MD	PFC	-	Contralateral hemisphere, GCC, Caud, MFG, IFG, BCC, MFG
TR6	PN/CN	PrCG	-	Contralateral hemisphere, SCC, BCC, Ins, PoCG, SFG, MFG, IFG
TR7	PN/CN	PFC	-	Contralateral hemisphere, GCC, BCC, ACC, IFG, MFG
TR8	PUL	AG	-	Contralateral hemisphere, SCC, MOG, MTG, STG, SMG, PrCu, SOG, IOG
TR9	PUL	IOG	-	Contralateral hemisphere, SCC, MOG, LG, MTG
TR10	PUL	ITG	-	Contralateral hemisphere, Put, FU, STG, MTG, CGH, CP
TR11	PUL	LG	-	Contralateral hemisphere, cerebellum, IOG, FU, MOG, ITG, PCC, SCC
TR12	PUL	MOG	-	Contralateral hemisphere, SCC, MTG, LG, IOG, CU
TR13	PUL	MTG	-	Contralateral hemisphere, AG, STG, ITG, Hippo, CGH, SCC, Amyg, IOG, FU, STG
TR14	PUL	SMG	-	Contralateral hemisphere, STG, MTG, AG, SPG, PoCG
TR15	PUL	SPG	-	Contralateral hemisphere, SCC, AG, PrCu, PoCG
TR16	PUL	STG	-	Contralateral hemisphere, Put, Ins, ITG, FU, SMG, AG, IOG, PrCG, PoCG, Amyg, MOG
TR17	VA	SFG	-	Contralateral hemisphere, Caud, IFG, BCC
TR18	VA	IFG	-	Contralateral hemisphere, Put, STG, MFG, SFG, PrCG, LFOG, Ins

Tract Name	1 st ROI	2 nd ROI	Waypoint ROI	NOT ROIs
TR19	VA	MFG	–	Contralateral hemisphere, Put, IFG, SFG, STG, PrCG, Caud
TR20	VL	PrCG	–	Contralateral hemisphere, BCC, SCC, Ins, PoCG, SFG, Put, STG, MTG
TR21	VL	SFG	–	Contralateral hemisphere, IFG, SOG, BCC, SMG, PrCG
TR22	VP	PoCG	–	Contralateral hemisphere, SCC, PCC, SMG, STG, IFG, PrCG, ACC
CST	CST	PrCG	–	Contralateral hemisphere, STG, MTG, ITG, IFG, PoCG, SPG
CPT1	CP	AG	–	Contralateral hemisphere, ITG, MOG, SCC, SOG, SMG
CPT2	CP	CU	–	Contralateral hemisphere, cerebellum, SPG, PrCU, PCC, SCC, SOG, LG
CPT3	CP	FU	–	Contralateral hemisphere, cerebellum, SCP, MCP, SPG, PrCU, PCC, SCC, MOG, LG
CPT4	CP	IFG	–	Contralateral hemisphere, Put, STG, MFG, PrCG, MGF, PrCG, LFOG
CPT5	CP	IOG	–	Contralateral hemisphere, cerebellum, SCP, MCP, ITG, FU, AG, SCC
CPT6	CP	ITG	–	Contralateral hemisphere, MCP, cerebellum, Hippo, CGH, MTG, FU
CPT7	CP	LG	–	Contralateral hemisphere, SCC, PCC, CU, Midbrain, SCP, MCP, CGH, Hippo, Thal
CPT8	CP	MFG	–	Contralateral hemisphere, LFOG, Put, ITG, STG, MTG, IFG, PrCG, SFG
CPT9	CP	MOG	–	Contralateral hemisphere, SCP, MCP, MTG, SCC, LG, STG, ITG, SCC, Hippo, CGH, IOG, SOG, AG
CPT10	CP	MTG	–	Contralateral hemisphere, AG, STG, ITG, FU, MOG, MCP, SOG, IOG
CPT11	CP	PoCG	–	Contralateral hemisphere, STG, MTG, ITG, AG, MOG, IOG, MCP
CPT12	CP	SFG	–	Contralateral hemisphere, GCC, BCC, MFG, Caud, ACC
CPT13	CP	SMG	–	Contralateral hemisphere, AG, STG, ITG, MTG, PoCG
CPT14	CP	SPG	–	Contralateral hemisphere, SCC, CGH, PCC, SOG, MOG, AG, PoCG
CPT15	CP	STG	–	Contralateral hemisphere, MTG, ITG, MFOG, IFG, LFOG, MCP, Ins, Put, PoCG, SMG

*, 1st ROI and 2nd ROI were two seed ROIs defining the beginning and end area of the tract. Waypoint ROI indicate the areas where fibers have to penetrate. “NOT” ROIs were defined to remove frequently-happening false positives. Fiber types were indicated by the different text colors (blue - commissural; tan – thalamic radiation; red – cortico-spinal tract; green – cortico-pontine fibers).